PROCEEDINGS of the
23rd International Congress on Acoustics

9 to 13 September 2019 in Aachen, Germany

Measurement and simulation of vibration acceleration of a high voltage three-phase gapped-core reactor

BART VAN DER AA[1]; BART WIJNHOVEN[1]; TIMO OVERBOOM[1]; LUC DORPMANNS[1]

[1] Royal SMIT Transformers (SGB-SMIT Group), Large Power Transformers, Nijmegen, The Netherlands

ABSTRACT

In this work, vibration acceleration of a high-voltage three-phase gapped-core shunt reactor is studied. The active part is oil-immersed, has three wound limbs, and two flux return limbs. Measurements are done using fibre optical accelerometers, which allows one to install sensors at locations otherwise not accessible for conventional piezoelectric accelerometers due to presence of high electromagnetic fields. Measured results are compared to simulation results, where forcing of the structure is assumed to be dominated by Maxwell forces. The study shows good qualitative agreement at twice the power frequency. Results obtained give insights in the dynamic behaviour of the gapped-iron core, which can be used for optimization of noise and vibration behaviour.

Keywords: Power Transmission, Shunt Reactor, Gapped-Core Reactors, Vibration, Maxwell forces, Fibre Optical Sensors

1. INTRODUCTION

Gapped core reactors are electrical components mainly used in electrical transmission networks. Their function is to stabilize the grid voltage by consuming reactive power of overhead lines in low load conditions, e.g. during night time. High quality and long term stability of such components is crucial for a reliable transmission network, but next to that low noise and vibration levels are often required by customers. The current trend is that even lower noise and vibration levels than today's standard are requested, and all manufactures are confronted to meet these challenging demands.

Noise emission by gapped-core shunt reactors and other electrical components such as (large) power transformers has a tonal character. This can be perceived as more annoying than broadband noise with the same equivalent sound levels (1). Primary sources of noise and vibration of gapped-core reactors are linked to the iron-core and current conducting windings. Three different source mechanisms can be distinguished: i) Lorentz forces acting on the windings, ii) Maxwell forces at the interface between core-steel and air, and iii) magnetostriction which is a property of all ferromagnetic materials. Because all phenomena are simultaneously present the determination of the main source of vibration and noise can be challenging. In various studies, researchers came to the conclusion that for some designs core vibration is dominated by Maxwell forces (2), whereas for other configurations magnetostriction dominates the response at twice the power frequency (3). Further, it was shown that for a two-legged gapped core reactor with a small gap, i.e. approximating an ordinary transformer core, magnetostriction dominates the overall vibration response, but by increasing the total gap length the Maxwell force component will increase and eventually dominates the overall response (4). In (5) a direct comparison was made between two cores of the same global dimensions, where an gap of 2 mm was created in the middle limb of one core. It was found that the peak-to-peak vibration acceleration of the reactor core was three times higher than the transformer core, which can be attributed to Maxwell forces (5). The optimal choice of spacer material, i.e. the non-conducting material which create the gaps, was also investigated in relation to noise and vibration. In (6) it was shown that optimizing the modulus of elasticity of the spacers can significantly lower the vibration response, which was also reported in (2).

[1] bart.van.der.aa@sgb-smit.group

It should be noted that the above mentioned results are obtained for model scale cores operated at a few hundred volts maximum. The active part of these reactors is therefore surrounded by air, as opposed to high voltage equipment where oil is normally used as di-electric insulation and cooling medium. The dynamic mechanical response of a structure immersed in oil will however be modified by a fluid loading phenomenon in such a way that the natural frequencies are altered from their in-vacuum values (7). In addition, it can be shown that model scale cores with length scales in the order of decimetres have eigen-frequencies at higher frequencies than high-voltage units where length-scales are in the order of meters. Tank vibrations and sound levels of an oil-immersed high-voltage single phase gapped-core reactor was studied in (8). It was reported that the eigen-frequency of the so-called the box-mode was altered by 10 Hz due to fluid loading (8), which shows that a fully coupled analysis is needed when considering an oil-immersed active part. Further, it was reported that Maxwell forces are the dominant source of vibration in (high-voltage) reactors (9). Direct comparison of the measured and simulated on-load vibration response has, to the best of our knowledge, not been reported for high-voltage oil-immersed shunt reactors.

In this work, vibration acceleration of a high-voltage three-phase gapped-core shunt reactor is studied numerically and experimentally. Simulation results are compared against measured results at twice the power frequency. It is assumed that core vibration is dominated by Maxwell forces, which implies that magnetostriction is neglected in the numerical analysis. Measured results are obtained using fibre-optical sensors, which allows one to install sensors at locations otherwise not accessible for conventional piezoelectric accelerometers. The reactor considered is a three-phase, five-legged design with a nominal voltage of 400 kV, and 150 MVAr reactive power. Its oil-filled weight is in the order of a few hundred metric tons, and typical length scales of the active part are in the order of meters in all directions.

2. THE MODEL

2.1 Basic Description of a Gapped-Core Reactor

A gapped-core reactor basically consist of a magnetic iron-core with current conducting windings. In case of a fixed power reactor, each phase is equipped with a single winding, but designs with multiple windings per phase are also possible and are referred to as variable power shunt reactors (VSR's). Depending on the application and design philosophy a single or three-phase concept is used, where the latter can have three or five limbs. With a five limb layout, which is studied here, the outer two approximately rectangular limbs are referred to as flux return limbs. The wound limbs, on the other hand, are cylindrically shaped and built up by radially stacked packets, see Figure 1.

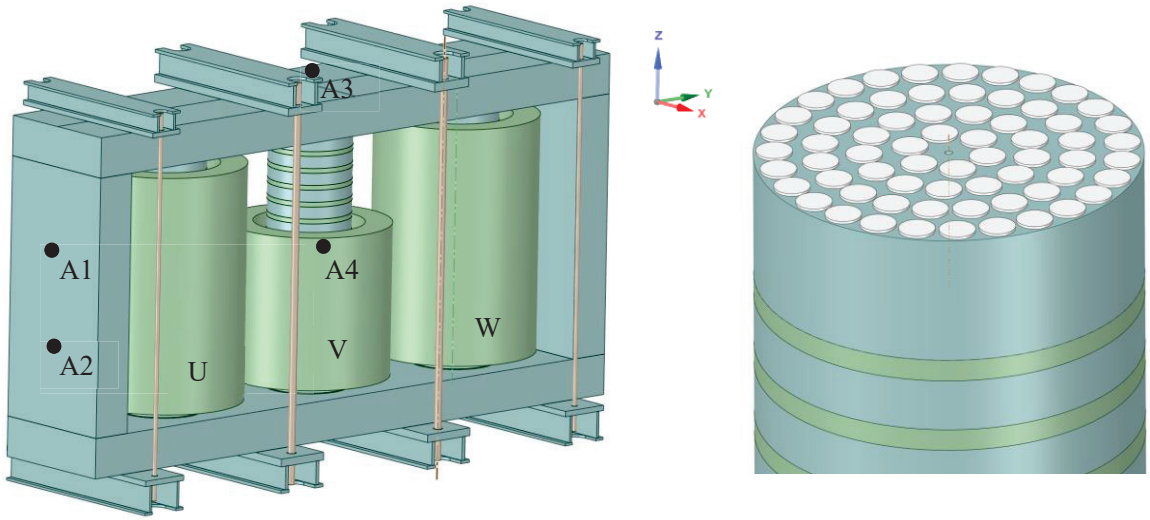

Figure 1: Illustration of three-phase 5-legged gapped-core active part (left), and close-up of a gapped-core limb with steatite spacer discs (right).

Between the three phases the magnetic flux is carried by the top- and bottom yokes. Together with

the flux return limbs the yokes form a low reluctance path for the magnetic flux. The radially stacked core packets are separated by non-magnetic steatite disks, which create the gaps. The total gap created is an important design parameter of a gapped-core reactor and mainly determines, next to the cross-sectional area of the limb, the impedance of the device. The core is built up from thin sheets of grain-oriented electrical steel and can contain thousands of laminations per sub-component. The assembled yokes and flux return limbs gain its stability and stiffness from a clamping construction which acts in the direction of lamination (not shown here). Such a laminated structure is very strong and can withstand large in-plane loads. This property is needed, as the forces to clamp the gapped-core limbs and windings are transferred from the tie-rods to the bridges to the yokes. A well-balanced pressure exerted on the gapped-core limbs is needed to minimize vibration levels due to high dynamic forces acting on the core.

2.2 Electromagnetic Force Model

It is assumed that vibration at twice the power frequency of a high-voltage gapped-core reactor is dominated by Maxwell forces, which can be interpreted as attractive forces that try to minimize the gap length. In order to calculate the Maxwell forces that act on the individual core-packets a two-dimensional axis-symmetric electromagnetic model based on Rabin's method is utilized (10). The magnetostatic harmonic model gives an analytical solution to the 2d-vector potential A in the rz-plane, by solving a truncated set of boundary conditions. Using $A(r,z)$ the axial component of the flux density B_z, and the radial component of the flux density, B_r can be obtained. Using the computed B-field, peak axial forces, F_z, are here calculated at the top and bottom surface of each packet and yoke:

$$F_z = \pm\pi \int_0^R \frac{B_z(r)^2}{u_0} r\, dr,$$

where, u_0 is the magnetic permeability in vacuum, and R the radius of the gapped-core limb.

In the context of this work, results are obtained for a fictive single-phase configuration, where geometrical properties of one gapped-core limb with yokes and flux return limbs, are taken into account. Hence, it is assumed that three-dimensional effects have only a marginal impact on the computed Maxwell forces acting on the surface of each core-packet, which has been verified by comparing three-dimensional simulations using *Ansys Maxwell*. It was found that the difference between the computed peak forces of the analytical approach and 3D-FEM was maximum 10%, where the analytical approach typically results in a somewhat higher value. The same discrepancy between analytical and numerical results were reported in (8).

The computed normal forces acting on the top- and bottom surfaces of the gapped-core packets are shown in Figure 2.

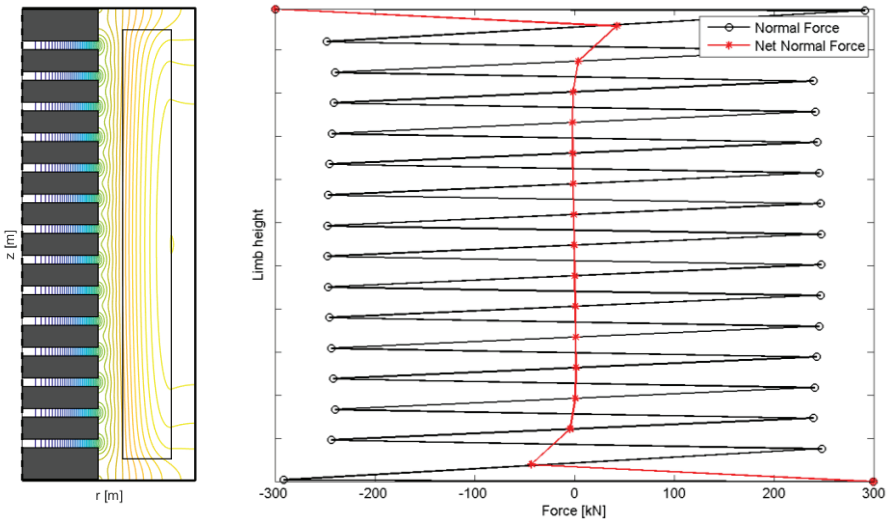

Figure 2: Flux lines (left), and axial forces acting on the gapped-core limbs and yokes (right). Positive forces are linked to the top faces of the packets, whereas negative forces are linked to the bottom faces.

In addition, the net normal force acting on the individual packets are also shown. It can be seen that forces acting on the top- and bottom faces of an isolated packet are in opposite direction and have approximately the same magnitude, resulting in a near-to-zero net force acting on each packet. This holds, except for the two outer most packets, where a difference in gap-height and geometrical configuration ultimately leads to a deviation of the axial force component of the top and bottom faces. Further, it can be seen that the forces between the yokes and end-packets are biggest, and the peak values are in the order of a few hundred kilo newton for this configuration. The direction of these forces is always inwards, i.e. the normal forces are pointing towards the geometrical centre of the structure, at half-height of the limb.

2.3 Vibroacoustic Model

To simulate the vibration response of a gapped-core active part, a fully coupled vibroacoustic harmonic model is setup in *Ansys Workbench*. Details about the setup and main assumptions are discussed below.

2.3.1 Mechanical Model

The active part of the gapped-core reactor is immersed in oil and enclosed by the reactor tank. The stiffened tank structure is geometrically simplified by leaving out e.g. the bushings, the conservator tank, and radiators. In addition, small-scale details such as flanges, control-cabinets, and other accessories are also left out. This will by definition have an effect on the eigen-frequencies of the complete system, but as measurements are performed on the active part, the impact to the simulated response is considered minor.

The solid mechanical model, i.e. all non-fluid domains, comprises of three basic materials. The components forming the tank are modelled as construction steel with a density of $\rho = 7850$ kg/m3, Young's modulus of $E = 2\text{e}11$ Pa, and a Poisson's ratio of $\upsilon = 0.3$. All core steel components, i.e. yokes, limbs and return limbs, are assumed to have isotropic properties with a density of $\rho = 7650$ kg/m3, a Young's modulus of $E = 1.1\text{e}11$ Pa, and a Poisson's ratio of $\upsilon = 0.3$. The non-magnetic steatite spacer disks are assumed to have a density of $\rho = 2650$ kg/m3, a Young's modulus of $E = 7\text{e}10$ Pa, and a Poisson's ratio of $\upsilon = 0.24$. To reduce computational efforts and minimize small scale details in the computational mesh, regions with steatite spacer disks are substituted by an homogeneous cylinder with equivalent material properties E_{eff} and ρ_{eff}, as suggested in (7). Practically speaking more material is introduced, which is compensated by lowering the Young's modulus and density through multiplication with the filling factor of the air-gap, ff, being 0.55 in this case.

In this paper, it is further assumed that the active part and tank are only coupled via the enclosed fluid, which means that direct structural coupling paths are neglect in the analysis. The active part is fixated in the fluid domain by imposing a *fixed* support condition at the imprint faces of the lower support bridges. Other components to pre-stress the structure, i.e. upper bridges and tie-rods, are also omitted from the analysis.

2.3.2 Mechanical Excitation

The structure is mechanically excited by the calculated Maxwell forces as described in section 2.2, which are imported as nodal forces acting on the top- and bottom surface areas of each gapped-core packet. The applied force is divided by the number of nodes, which effectively results in a homogeneous force distribution. Further, it shall be noted that the Maxwell forces are proportional to the squared values of B_z, which implies that for a harmonically oscillating B-field, the resulting force is non-zero crossing. In other words, the polarity of the force is not changing during a full (sinusoidal) period of the applied magnetic field. Using a harmonic solver, applied loads are by nature of the method oscillating around zero, and hence polarity of the force vectors are changing after half a period of the excitation frequency. To simulate the true, non-zero crossing force function, a transient solver has to be used. However, the same acceleration response can be obtained by using a harmonic solver if the peak amplitude of the harmonic force function is set to $F_z/2$, which is utilized here.

In a three-phase AC-system the U, V, and W lines will produce an equal magnitude voltage with an equally spaced mutual phase angle at +/- 120° form a reference line at a given frequency. The instantaneous Maxwell forces acting on the three gapped-core limbs also experience the same phase shift. However, as the axis-symmetric electromagnetic model is only laid out for a single phase

configuration no (computed) mutual phase information is available. Here, forces applied to the U, V and W phases are given an exact mutual phase-shift of 120˚.

2.3.3 Fluid Structure Interaction

Having a vibrating structure surround by a heavy fluid such as oil, the response of the system is altered due to a fluid-loading phenomenon. In the simplified case that pressure waves radiate to infinity and do not reflect back on the surface of the structure, the fluid exerts a constant force field to the structure which can be seen as an added mass. However, when the fluid is contained by e.g. a tank, acoustic waves reflect upon the boundaries and can interfere with intersecting pressure waves, which may lead to acoustic modes. From literature it is known that a contained fluid exhibits a resonant acoustic behaviour, producing a strongly frequency dependent response (7). This, in combination with a narrowband excitation mechanism is best solved by a fully coupled formulation.

Coupling of the structural domains and the fluid domain is done at the outside surfaces of the core and inside surfaces of the tank. To do that, two coupling boundary conditions are imposed. The first coupling condition states that vibration velocity of the mechanical structure normal to the surface shall match the surface normal velocity of the fluid, whereas the second coupling condition states that an acoustic pressure wave will introduce mechanical stress to the solid. The combination of the first and second coupling condition assures a feedback mechanism, which enables vibrational energy to be transferred to acoustic energy and back to vibrational energy again.

In this work, the speed of sound in oil is assumed to be 1400 m/s, whereas the density of oil is assumed to be 850 kg/m3.

3. MEASUREMENTS

On-load vibration measurements of the gapped-core shunt reactor has been performed in the high-voltage laboratory of Royal SMIT Transformers. To energize the reactor at rated voltage and rated current the unit has been connected to a step-up transformer.

To measure on-load vibration of high-voltage electrical components, ordinary piezo-electrical accelerometers which are resistant to oil, solvents and other liquids are available on the market. However, the drawback is that these piezo-electrical sensors are sensitive to external magnetic fields, and their co-axial cables cannot be routed through zones where high electrical field strengths are present. To mitigate these shortcomings custom-made single-axis fibre-optical accelerometers have been implemented, which are manufactured from non-magnetic non-conducting materials.

The basic principle of the fibre-optical vibration measurement technique used here is to track the dynamic displacement of an optical resonator. By application of a given vibration signal the sensor response will exhibit a continuous shift of the measured optical resonance peak around a known optical resonance frequency. In a post-processing step the transient optical displacement response of each sensor is translated into a transient acceleration signal, which in a second post-processing step is translated to the frequency domain using FFT. A vibration acceleration level is than obtained through $VAL = 20\log_{10}(|a|/a_0)$, where a is the measured acceleration, and a_0 is the reference acceleration here set to 1e-6 m/s^2.

Here, four single-axis fibre-optical accelerometers have been fixed to the active part of the gapped-core reactor, see Figure 1 for the schematic locations. Sensors A1 and A2 are mounted to the flux return limb, with their principle measurement axis placed parallel to the y-axis of the global domain, which is shown in Figure 1. Sensors A3 and A4, on the other hand, have their principle measurement axis placed parallel to the z-axis. An example of a fibre-optical accelerometer mounted on the gapped-core limb is shown in Figure 3.

Now, energizing the reactor at 50 Hz will lead to Maxwell forces at twice the power frequency, i.e. 100 Hz in this case. In absence of other excitation mechanisms, the measured vibration response will display a distinct peak at 100 Hz similar to the one shown in Figure 3.

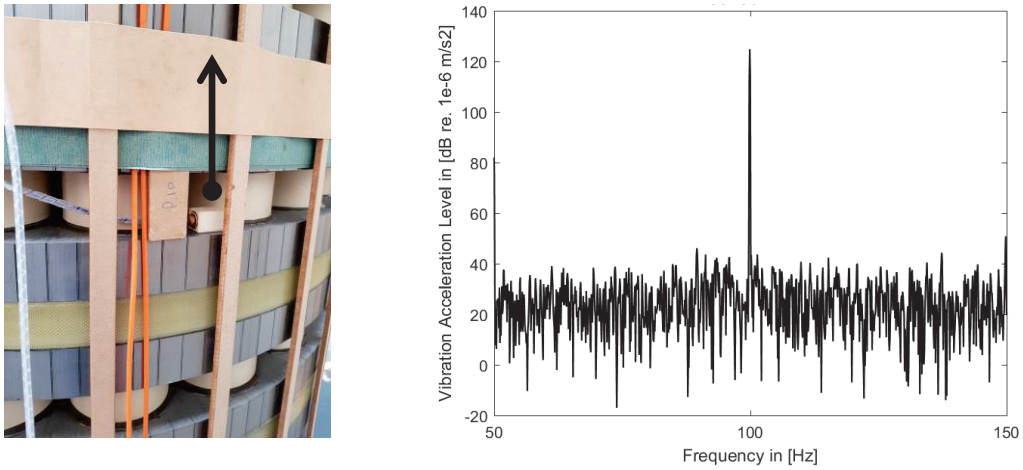

Figure 3: Fiber-optical acceleration sensor at outer edge of gapped-core packet (left). typical response spectrum for a system operated at 50 Hz power frequency (right).

4. RESULTS

4.1 Simulated Forced Response

The total, and y-component, of the modelled vibration acceleration at 100 Hz with phase angles of 0˚ and +180˚ are shown in Figure 4. It can be seen that phase U at 0˚ phase angle displays a peak in total acceleration, and simultaneously the neighbouring flux return limb exhibits its maximum acceleration with positive slope in the y-direction. This happens when the applied force field to phase U is at its maximum and is pointing inwards. Now, at +180˚phase angle the flux return limb has its maximum acceleration with negative slope, which happens when the force field is at its minimum and is pointing outwards. In both cases, the flux return limb next to phase W experience only a very small acceleration. The acceleration of the flux return limb next to phase W is at is maximum at approximately +90˚ and +270˚ phase angle. Due to the three-phase excitation mechanism the vibration response appears to travel from phase W to phase U, which obviously would be revered by swapping the phase angles of the both phases. The oil pumping effect of the flux return limb is considered to be an important source of transmitted vibrations to the tank, as was also addressed by (8).

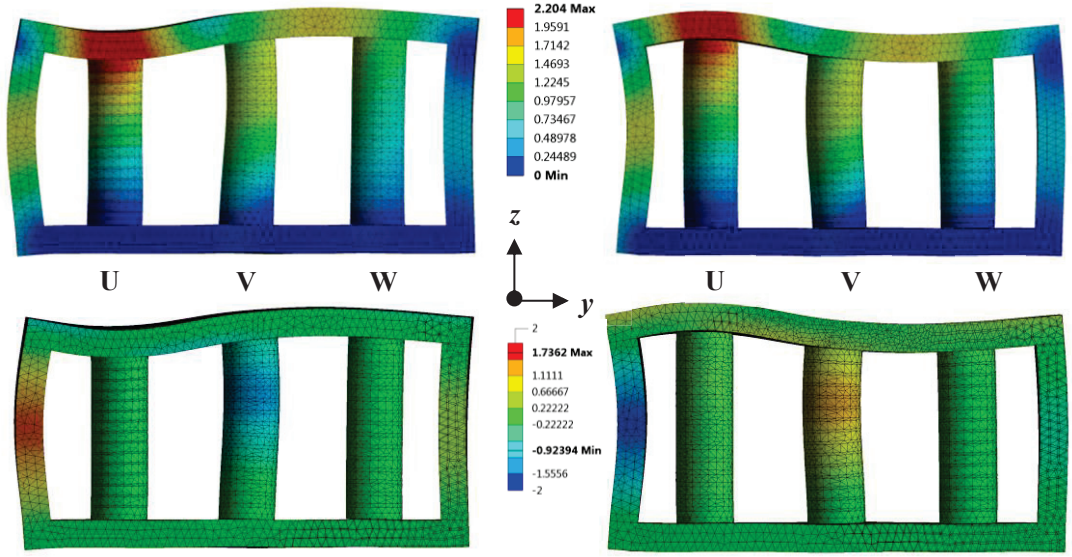

Figure 4: Total vibration acceleration of gapped-core reactor at 100 Hz and a phase angle of +0˚ (top-left), and +180˚ (top-right). Vibration acceleration, y-component , at 100 Hz and a phase angle of +0˚ (bottom-left), and +180˚ (bottom-right). The acceleration response is projected on a deformed frame.

4.2 Multiple Frequency Excitation

With a fine enough spatial resolution it is possible to visualize the measured operational deflection shape at the driving frequency. This is not possible with the set of accelerometers used here. However, to display the underlying mechanical response at the measurement locations, it is possible to drive the system at a variable frequency with constant force. This can be done by means of a constant frequency approach, i.e. by treating each frequency as a separate test. In this work, a discrete multiple frequency excitation is executed in a range from 48 to 52 Hz in steps of 1 Hz. This results in Maxwell forces appearing at 96 to 104 Hz in steps of 2 Hz.

The measured vibration acceleration levels of sensors A1 to A3 are compared against the simulated vibration acceleration in Figure 5. To give an impression of the response outside the measured range, the simulated frequency range has been extended to +/- 10 Hz around the 100 Hz frequency component. It can be seen that the simulated response is in the order of 6 dB higher than the measured values, which holds for all three sensor locations. Further, it can be seen that the overall increasing trend with frequency is captured well.

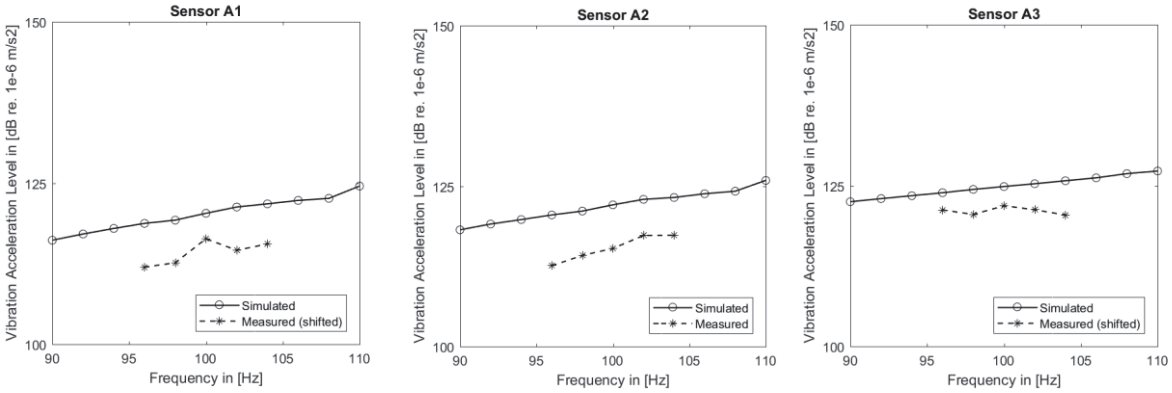

Figure 5: Comparison of measured and simulated Vibration Acceleration Levels at locations A1 to A3.

As phase information is not available between individual measurements, e.g. using a continuous reference signal, comparing the computed and simulated phase angles for a given sensor is not possible. By comparing the transfer functions between different sensors, the mutual phase lag can however still be recovered. The computed and measured phase difference from A1 to A3, and A1 to A2 are shown in Figure 6. As sensors A1 and A2 are both located on the flux return limb it is expected that the phase difference is small, which is confirmed by the measurements. The simulated angular difference from A1 to A2 is approaching zero, suggesting the model results are nearly symmetric about the middle axis. Comparing the computed and simulated angular difference from A1 to A3 it can be seen that measured results tend to +180˚, whereas the model predicts an angular difference of approximately +120˚.

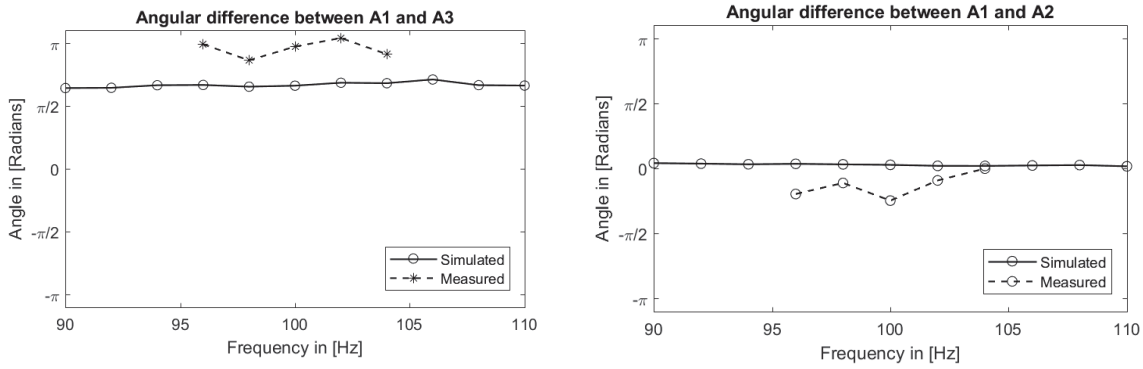

Figure 6: Measured versus simulated angular difference between sensor A1-A3 (left), and A1-A2 (right).

5. CONCLUSIONS

Vibration acceleration of a high-voltage three-phase gapped-core shunt reactor was studied in this work. Measurements obtained by fibre-optical accelerometers were compared to simulation results, where forcing of the structure was assumed to be dominated by Maxwell forces. The study shows good qualitative agreement at twice the power frequency for a small range of measured frequencies around the 50 Hz component. The fibre-optical technique has proven to give valuable insight in the dynamic mechanical behaviour of a three-phase gapped-core shunt reactor, which can be used for optimization of noise and vibration behaviour.

REFERENCES

1. Lee J. The Effects of Tones in Noise on Human Annoyance and Performance. University of Nebraska - Lincolm, U.S.; 2016.
2. Iamamura B, Rossi M, Hecquet M, Lanfranchi V, Recorbet S, Tridon F. Vibration and acoustic noise of industrial reactors associated to converters in railway domain: design and material impacts. COMPEL International Journal of Computations and Mathematics in Electrical. 2016;35(6):12.
3. Gao Y, Muramatsu K, Hatim MJ, Fujiwara K, Ishihara Y, Fukuchi S, et al. Design of a Reactor Driven by Inverter Power Supply to Reduce the Noise Considering Electromagnetism and Magnetostriction. IEEE Transactions on Magnetics. 2010 Jun;46(6):2179–82.
4. Rossi M, Le Besnerais J. Vibration Reduction of Inductors Under Magnetostrictive and Maxwell Forces Excitation. IEEE Transactions on Magnetics. 2015 Dec;51(12):1–6.
5. Zhang X, Yao X. Experiments and simulations on the vibration of shunt reactor and the noise control. . Vol. 2005;43:6.
6. Gao Y, Nagata M, Muramatsu K, Fujiwara K, Ishihara Y, Fukuchi S. Noise Reduction of a Three-Phase Reactor by Optimization of Gaps Between Cores Considering Electromagnetism and Magnetostriction. IEEE Transactions on Magnetics. 2011 Oct;47(10):2772–5.
7. Fahy F, Gardonio P. Sound and structural vibration: radiation, transmission and response. 2nd ed. Amsterdam ; Boston: Elsevier/Academic; 2007. 633 p.
8. Daneryd A, Olsson K, Bengtsson C. Tank vibrations and sound levels of high voltage shunt reactors; - advances in simulation methodologies. In Cracow, Poland: Cigre; 2017.
9. Anger J, Bengtsson C, Forslin J, Olsson K. An Innovative Concept for Noise Control of Shunt Reactors. In Brugge, Belgium: Cigre; 2007.
10. Rabins L., Transformer Reactance Calculation with Digital Computers; Transactions of the American Institute of Electrical Engineers, Part I: Communication and Electronics. 1956; 75(3):261-267